Biochimica et Biophysica Acta 854 (1986) 45–57
Elsevier

BBA 72851

One-dimensional crystals of $(Na^+ + K^+)$-ATPase dimers

G. Zampighi [a], S.A. Simon [a,*], J. Kyte [b] and M. Kreman [a]

[a] *Department of Anatomy and Jerry Lewis Neuromuscular Research Center, UCLA School of Medicine, Los Angeles, CA 90024, and* [b] *Department of Chemistry, D-006, University of California, San Diego, La Jolla, CA 92093 (U.S.A.)*

(Received August 5th, 1985)

Key words: $(Na^+ + K^+)$-ATPase crystal; Freeze-fracture; Electron microscopy; (Canine kidney)

Preparations of purified $(Na^+ + K^+)$-ATPase contain both fragments of membranes and long and undulating cylindrical structures. These structures have been described as edgeways of membrane fragments. We have analyzed these structures using negative staining, thin sectioning and freeze-fracture-etch electron microscopy and describe their structure for the first time. Each cylinder is 12–19 nm in width and is comprised of an unstained core from which rows of distinct particles spaced 5–6 nm apart project on both sides. Each cylindrical structure was interpreted as a linear polymer of $(\alpha\beta)_2$ dimers of $(Na^+ + K^+)$-ATPase molecules. Therefore, the particles that project from both sides are the cytoplasmic domains of the molecules of the enzyme, whereas the membrane-spanning domains form the unstained core of the cylinder. From considerations of the packing of the dimers in the cylinder we conclude that the cross-sectional area of the cytoplasmic domain should be larger than that of the membrane-spanning domain. Our results are consistent with the hypothesis that the $(\alpha\beta)$ protomer is the native state of the enzyme. The $(\alpha\beta)_2$ dimers observed in the fractions are the result of a secondary aggregation process occurring during the purification procedure.

Introduction

Active transport of sodium and potassium ions across plasma membranes is catalyzed by the sodium and potassium ion activated adenosine triphosphatase ($(Na^+ + K^+)$-ATPase) [1]. The enzyme has been isolated from several tissues [2–5] and shown to be constructed from two subunits. One is a large relatively hydrophobic protein designated α, and the other is a smaller sialoglycoprotein, designated β [2]. Chemical cross-linking has established that the two polypeptides form a specific complex, the $\alpha\beta$ protomer, whose total molecular weight is about 170000 [6–8].

The oligomeric state of the enzyme within the membrane has been a subject of controversy. Studies by chemical cross-linking [9,10] and radiation inactivation [11,12] suggested that $(\alpha\beta)_2$ dimers form the native structure of $(Na^+ + K^+)$-ATPase. Another approach used to examine this issue has been to dissolve the membrane-bound enzyme in solutions of nonionic detergents and then study the soluble complexes that displayed $(Na^+ + K^+)$-ATPase activity. The protein molecular weight of these complexes has been estimated to be 380000 $\pm$ 21000 in solutions of Lubrol WX [13] and either 256000 $\pm$ 23000 [14] or 170000 $\pm$ 9000 [15] in solutions of octaethylene glycol dodecyl ether. Recently, Craig [16] suggested that some of the conclusions about the oligomeric nature of the enzyme in solutions of detergents were in error because of heterodispersity of the resulting enzyme-detergent complexes. Craig [17] also found that the smallest complex having $(Na^+ + K^+)$-

* Permanent address: Departments of Physiology and Anesthesiology, Duke University Medical Center, Durham, NC 27710, U.S.A.

Abbreviation: Tes, 2-((2-hydroxy-1,1-bis(hydroxymethyl)ethyl)-amino)ethanesulfonic acid.

ATPase activity was the $\alpha\beta$ protomer. A similar finding has been reported by Esmann [14] although this author proposed that the $(\alpha\beta)_2$ dimer is the stable form of the enzyme.

Although these experiments provided a description of the oligomeric nature of the enzyme in solutions of detergent, the dimers of the enzyme observed in the membrane-bound form by chemical cross-linking must also be explained.

This report describes the structure of cylindrical polymers formed from molecules of $(Na^+ + K^+)$-ATPase. They are found in purified preparations of the enzyme, in addition to the membrane fragments described previously [18–21]. Our studies seem to indicate that these cylindrical structures are linear polymers of $(\alpha\beta)_2$ dimers which seem to result from a rearrangement of the molecules during isolation. These presumably artifactual associations might explain why $(\alpha\beta)_2$ dimers are detected in preparations of the purified enzyme.

Materials and Methods

$(Na^+ + K^+)$-ATPase. The starting material for all of the preparations of $(Na^+ + K^+)$-ATPase was a microsomal fraction prepared from the medullas of canine kidneys by the method of Jørgensen and Skou [22] as slightly modified by Kyte [2]. These microsomes were further purified by treating them with the detergent sodium dodecyl sulfate (SDS) and then submitting them to isopycnic zonal centrifugation [3,21]. This procedure provided a series of fractions that differed in their buoyant density. Briefly, a mixture was prepared from the microsomes whose final concentrations were 2.0 $mg \cdot ml^{-1}$ protein, 2 mM Na_2ATP, 1 mM Na_2 EDTA, 0.6 $mg \cdot ml^{-1}$ SDS, 25 mM imidazolium chloride, pH 7.5 at 4°C. This sample was injected onto a continuous sucrose gradient (10–45%) and centrifuged for 150 min at 45000 rpm, in a Ti 14 zonal rotor. Only those fractions having a buoyant density of 1.31 ± 0.1 $g \cdot ml^{-1}$ had $(Na^+ + K^+)$-ATPase activity. The fractions were centrifuged separately and resuspended at 2–3 mg protein/ml in 0.25 M sucrose, 1 mM Na_2 EDTA, 0.1% 2-mercaptoethanol and 30 mM histidinium chloride, pH 7.1. The suspensions were divided into aliquots of 50 μl, frozen in a bath of solid CO_2 in isopropanol, and stored at −70°C.

We have observed the cylindrical polymers in $(Na^+ + K^+)$-ATPase fractions suspended in the solution used to store the membranes as well as in all the solutions of various ionic composition examined thus far [21]. These cylinders are found regardless of changes in the concentrations of Na^+ (0.5–10 mM), K^+ (1–10 mM), Mg^{2+} (5–120 mM), Ca^{2+} (0.5–5 mM), phosphate (1–5 mM), NH_4OH or vanadate (20–400 μM), or changes in pH from 5 to 8 with different organic buffers.

Thin sectioning. Suspensions of $(Na^+ + K^+)$-ATPase were fixed in a solution containing 4% glutaraldehyde, 0.3% tannnic acid, 0.1 M sodium cacodylate, pH 7.3. After 2 h at 4°C, the suspensions were placed on top of a piece of Millipore filter type VSWP, with its shiny side up. The piece of filter and the suspension were supported on an adapter that was cast from epoxy resin to fit into the bottom of a Beckman SW60 Ti rotor tube. The membranes were deposited by centrifugation at 20000 rpm for 90 min. The piece of filter was washed, postfixed in osmium tetroxide, and dehydrated in ethanol. The pellet and what remained of the filter were soaked in a mixture of equal volumes of ethanol and Epon 812 for 1 h, and passed through propylene oxide/Epon 812 mixtures and embedded in pure Epon 812 [23].

Sections exhibiting a gray interference color were cut with a diamond knife mounted on a MT-5000 Sorvall ultramicrotome and deposited on carbon-coated grids. The sections were triple-stained on the grids with uranyl acetate, lead citrate and bismuth subnitrate [24].

Negative staining. $(Na^+ + K^+)$-ATPase was deposited from suspension on freshly prepared carbon-coated grids. The grids were then washed with 1–2% uranyl acetate and photographed at ×40000 magnification, at minimum exposure with a microfocusing device. They were recorded sufficiently close to focus that the contact transfer function was uniform over the spacing of interest [25]. The microscopy was performed with either a Zeiss EM10C or an EM109 electron microscope at acceleration voltages of 80–100 kV. Tilt series of the cylinders were obtained in the goniometer stage of the microscope. The long axes of the cylinders were oriented parallel to the tilt axis by rotating the specimen in a rotating and tilting goniometer. The changes in magnification due to

small displacements of the specimen along the z-axis of the microscope were compensated for by recording the lens current and then using the correction factors recommended by the manufacturer. The negatives were studied by inspecting their optical transforms in a diffractometer constructed according to the model described by Salmon and DeRosier [26].

Freeze-fracture-etch. 50 μl of a suspension of $(Na^+ + K^+)$-ATPase, 2–3 mg protein/ml in 10 mM $MgCl_2$, 1 mM $MnCl_2$, 5 mM H_3PO_4, 25 mM Tes at pH 6.8, was centrifuged in an Eppendorf microfuge for 5 min. The resulting loose pellet was then fixed for 1 h with 4% glutaraldehyde in 0.2 M sodium cacodylate, pH 7.3. After fixation, the pellet was washed in distilled water for 2 h and trimmed to a size of $0.25 \times 0.25 \times 0.5$ mm. These pieces were placed on Balzers' holders, incubated in a chamber of 100% relative humidity for 3 min [24] and frozen in liquid propane with a guillotine-type device [28].

Freeze-fracture-etch was performed in an Edward 306 coater. The holders were transferred from liquid nitrogen to a specimen table cooled at −160°C. After a vacuum in the range of about $1 \cdot 10^{-6}$ mbar had been obtained, the temperature of the specimen table was raised passively to the temperature at which both fracturing and etching were carried out. The specimen was fractured with a knife cooled to liquid nitrogen temperature and the surface was etched at −105°C for times ranging from 15 to 90 s. The surface was replicated unidirectionally at 45° with platinum-carbon and at 90° with carbon.

Results

Negative staining

Fig. 1 shows a low-magnification view of a negatively stained preparation of $(Na^+ + K^+)$-ATPase isolated from canine renal medulla by the procedure of Jørgensen [3]. The fractions from which these views were obtained displayed the highest enzymatic activity and the highest purity as determined by polyacrylamide gel electrophoresis [18]. Fig. 1A shows several membrane fragments of irregular shapes and numerous cylindrical structures of constant diameter but variable length. The membrane fragments display a high density of enzyme molecules arranged in ordered rows spaced 5–6 nm apart. This type of lattice contains one $(\alpha\beta)$ protomer per unit cell and it has been previously described in detail by others [18–21]. These prominent structures were a constant component of all the fractions displaying enzymatic activity obtained from the isopycnic gradient, but they were present at greater frequency in the densest fractions displaying $(Na^+ + K^+)$-ATPase activity. The cylinders are not the product of the SDS purification step used in the Jørgensen method, since we also observed them in the microsomal preparation prior to the detergent treatment [2,22].

The cylindrical structures are seen either as short segments or long and undulating ropes. In either case, they can be continuous with the borders of the membranes or seen as independent entities. When the cylinders and the membranes are continuous with each other, they are always seen along the borders of the membrane fragments. The black arrows in Fig. 1A show the regions of transition between both structures. The transition is normally accomplished by a smooth tapering of a membrane edge into the cylinders.

In Fig. 1B three long (approx. 1 μm) cylindrical structures can be seen lying side by side. These long cylindrical structures have a constant width except in those regions where small pieces of membrane were associated with their sides (arrow Fig. 1B). Although the cylinders clearly stand out from the background, the regions between them give no indication of containing membranes. Consequently, the linear structures designated here as cylinders are not simply edge-on views of membrane fragments.

Each cylinder is comprised of an unstained core about 4 nm wide from which particles about 6 nm long and spaced 5–6 nm apart extend from both sides (Fig. 2A). The rows of particles seen on both sides of the core are slightly staggered, giving to the whole structure the appearance of a linear array of chevrons. The inset in Fig. 2A is the optical transform of the region of the cylinder located at the center of the figure. The diffraction pattern consists of sharp lattice lines, the most prominent of which have a spacing of about 5 nm^{-1} (arrow). These lattice lines arise from the repeating particles oriented nearly perpendicular

to the long axis of the cylinder. Note that the intensities along the lattice line spaced about 5 nm^{-1} are not symmetric with respect to the meridian. This feature is due to the uneven distribution of stain between the lateral surfaces of the cylinder. The angle at which the rows of particles are staggered with respect to each other was measured as about 10° from the distance between the maxima in the lattice line and the meridian.

Although the width of the cylinders appears constant in the low-magnification views, there is considerable variability when seen at higher magnifications. Fig. 2B shows this structural characteristic. The region labelled by the arrow displays an

Fig. 1. Low-magnification views of highly purified preparations of $(Na^+ + K^+)$-ATPase seen by negative staining. Several membrane fragments and numerous cylinders are shown in panel A. The black arrows denote junctions between these two structures. Three long cylinders that run almost parallel to each other in fairly straight paths are shown in panel B (opposite page). The arrow shows a region of a cylinder continuous with a small piece of membrane. Magnification: ×120000.

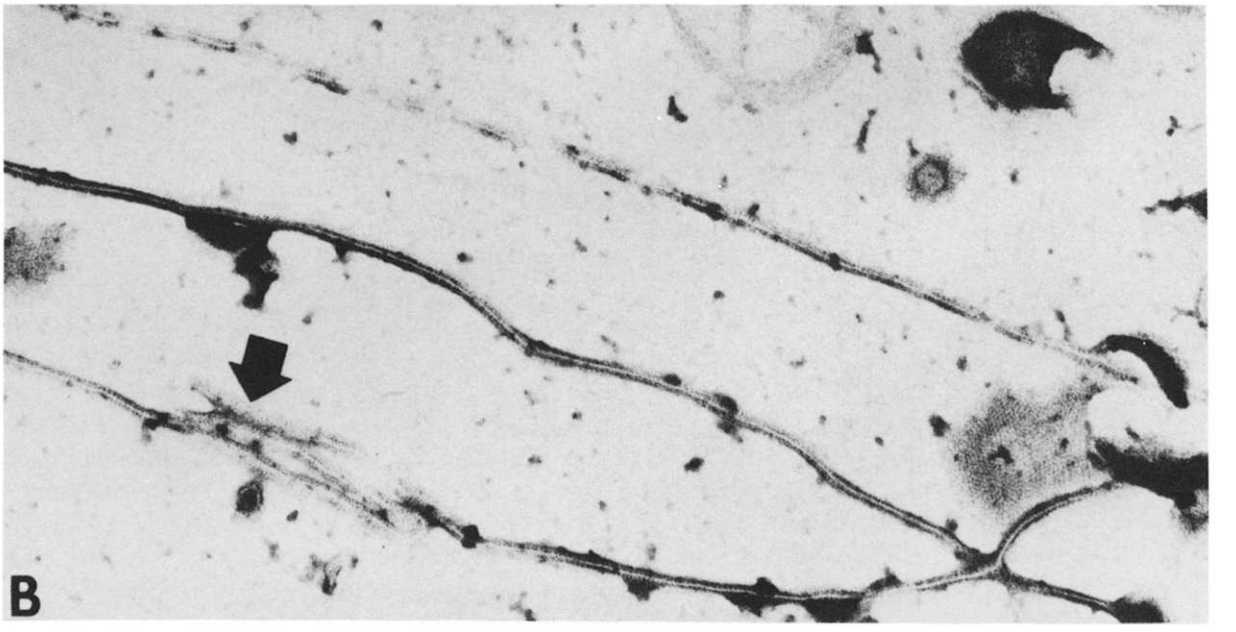

overall thickness of about 14 nm, whereas the lower portion of the cylinder in Fig. 2B is about 18–19 nm. This variability can be accounted for solely by changes in the width of the projection of the unstained core rather than by changes in the dimensions of the protruding particles. The arrow in Fig. 2B labels a region of the cylinder having a core about 4 nm wide, similar to that described previously in Fig. 2A. The regions of the cylinder located above and below the arrow in Fig. 2B, however, display cores about 9 nm in width with rows of particles protruding at both sides. Note that the continuity of the cylinder is maintained during this change in thickness and that pools of stain accumulate heavily at both sides of the region where the cylinder thins.

Additional details of the structural organization of these structures can also be discerned in the cylinders seen at high magnification. In Fig. 3A, the core is about 4–5 nm wide and from it distinct particles protrude on both sides. The particles are asymmetric, with dimensions of about 4 nm in diameter and about 6 nm in length (arrowheads in Fig. 3A and C). Upon close examination it is seen that the particles in these cylinders display several different projections. This variability may result from an interplay of factors such as the position of the protruding particles with respect to the viewing angle and the thickness of the layer of stain embedding the entire polymer. There are also particles that display a globular shape separated from the unstained core by a narrow band of stain. Occasionally (Fig. 3B), a cylinder displaying the same characteristics previously described, with well-defined cores and stalked particles extending from both sides, abruptly thickens, loses its characteristic unstained core and instead is covered with distinct particles. This thickened region displays the typical projection of molecules of $(Na^+ + K^+)$-ATPase observed in membrane fragments [29–32].

Fig. 3C shows a cylinder that displays projections along its minor axis (upper portion) and major axis (lower portion) as if it were twisted when deposited on the support film. Particles having different projections, particularly in the upper segments, can be found lying across the unstained core from each other. The particles labelled with the arrowheads at the left side are elongated in shape and can be followed to their insertion in the core. At the opposite side (open arrows), the particles are globular in shape. These particles are separated from the core by a narrow band of stain. The various projections of the particles can be accounted for if they are oriented at different angles with respect to the *z*-axis of the microscope.

Thus, the short protrusions that can be traced to the core (arrowheads in Fig. 3A and C) should be particles viewed obliquely to their long axis, while the spherical-shaped projections that are separated from the core by a thin layer of stain (open arrows in Fig. 3C) should arise from these particles viewed almost perpendicular to their long axis.

To obtain information about the overall shape and the orientation of the particles, the cylinders were tilted at different angles with respect to the incident electron beam about an axis parallel to their long axis. Fig. 4 shows selected views of a cylinder tilted from 0° to 30° in steps of 10°. The images of cylinders seen in Fig. 4 will be described with reference to changes in the organization of the particles and in the overall shape of the unstained core that arises from tilting the specimen in the microscope. A common view of the cylinder, in which the particles are better defined at one side (i.e., the left side, arrowhead) than at the

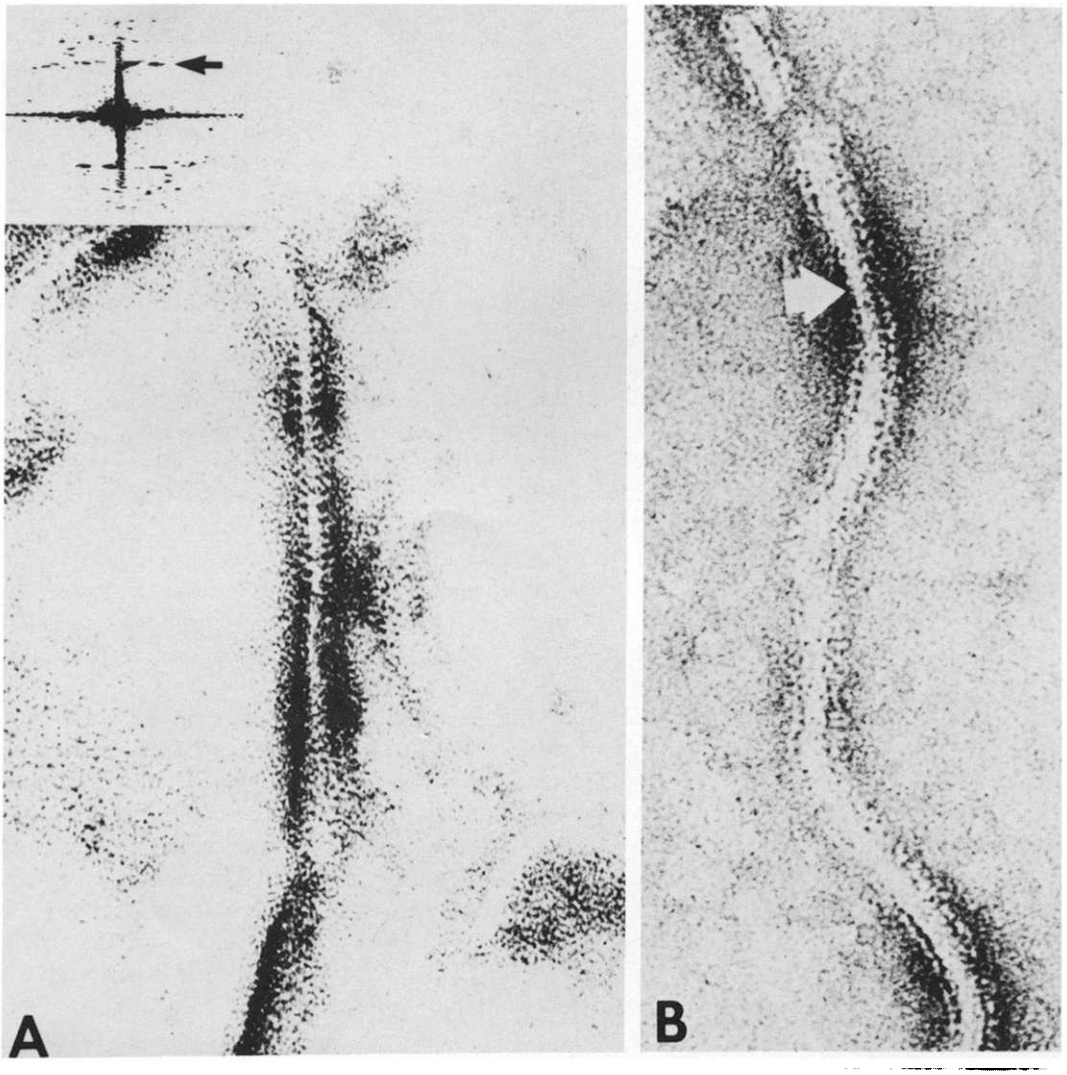

Fig. 2. A cylinder comprised of a core from which elongated particles protrude symmetrically is presented in panel A. The central portion of this cylinder was transformed optically and the pattern is presented in the inset. The black arrow in the inset points to a prominent layer line spaced at about 5 nm^{-1}. A long cylinder having its central core of variable thickness is shown in panel B. Magnification: ×400000.

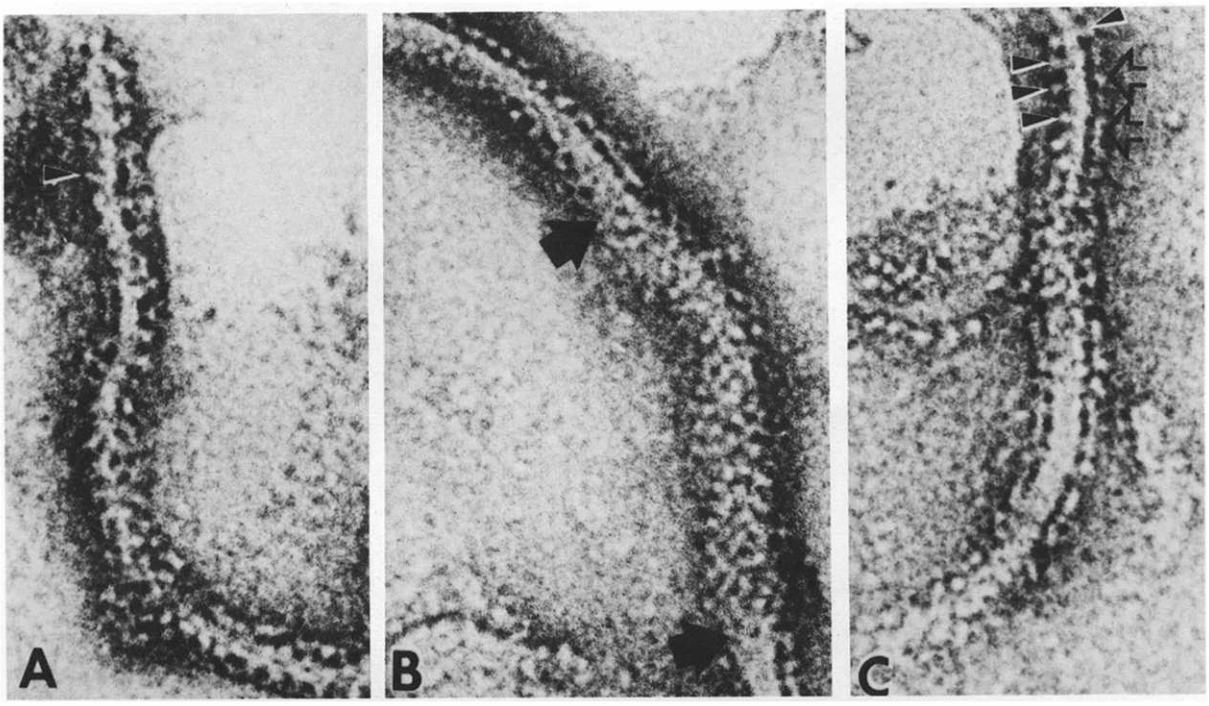

Fig. 3. Several structural details of cylinders at higher magnification. A thin cylinder in which the stalked particles can be resolved protruding from the central core in all directions is shown in panel A. The particles labelled with the arrowheads are protruding from the front surface of the core. They can be traced along their entire length to their insertion in the core. The abrupt change in the morphology of a cylinder that can occur along its length is displayed in panel B. The regions above and below the arrows have their central core and stalked particles clearly defined. The region between both arrows, however, is characterized by numerous particles spaced at about 5–6 nm apart and covering evenly the surface of the structure. A further demonstration of the variability in the width of the core that can occur along a cylinder is presented in panel C. The top portion of the cylinder is about 4 nm wide, whereas the lower portion is about 8 nm. Note the slightly different appearance of the particles protruding from the core at the top region. The particles labelled with arrowheads can be traced to their insertion in the front surface of the cylinder. Those particles labelled with open arrows appear globular and they are separated from the central core by a narrow layer of stain. Magnification: ×500000.

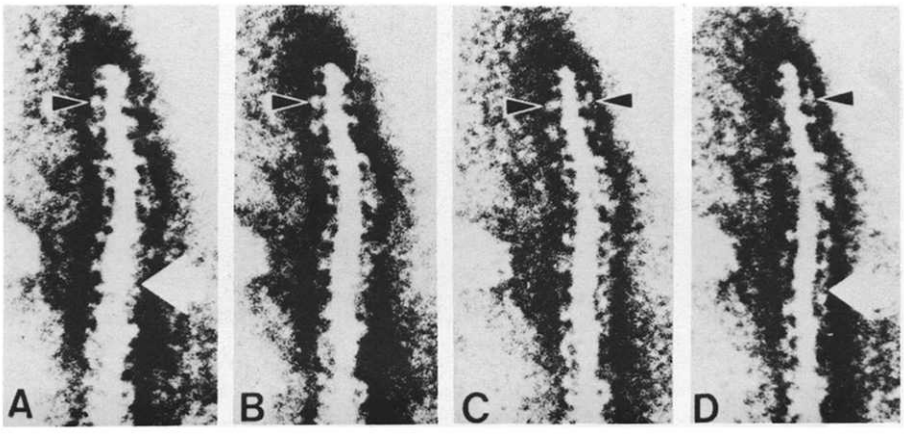

Fig. 4. Selected views from a tilt series of a cylinder that was oriented parallel to the direction of the tilt axis. Panel A = 0°, B = 10°, C = 20° and D = 30°. The arrowheads label particles that change their projected images as a function of the tilt axis. The black arrows indicate regions of the cores that became narrower as a result of tilting. Magnification: ×480000.

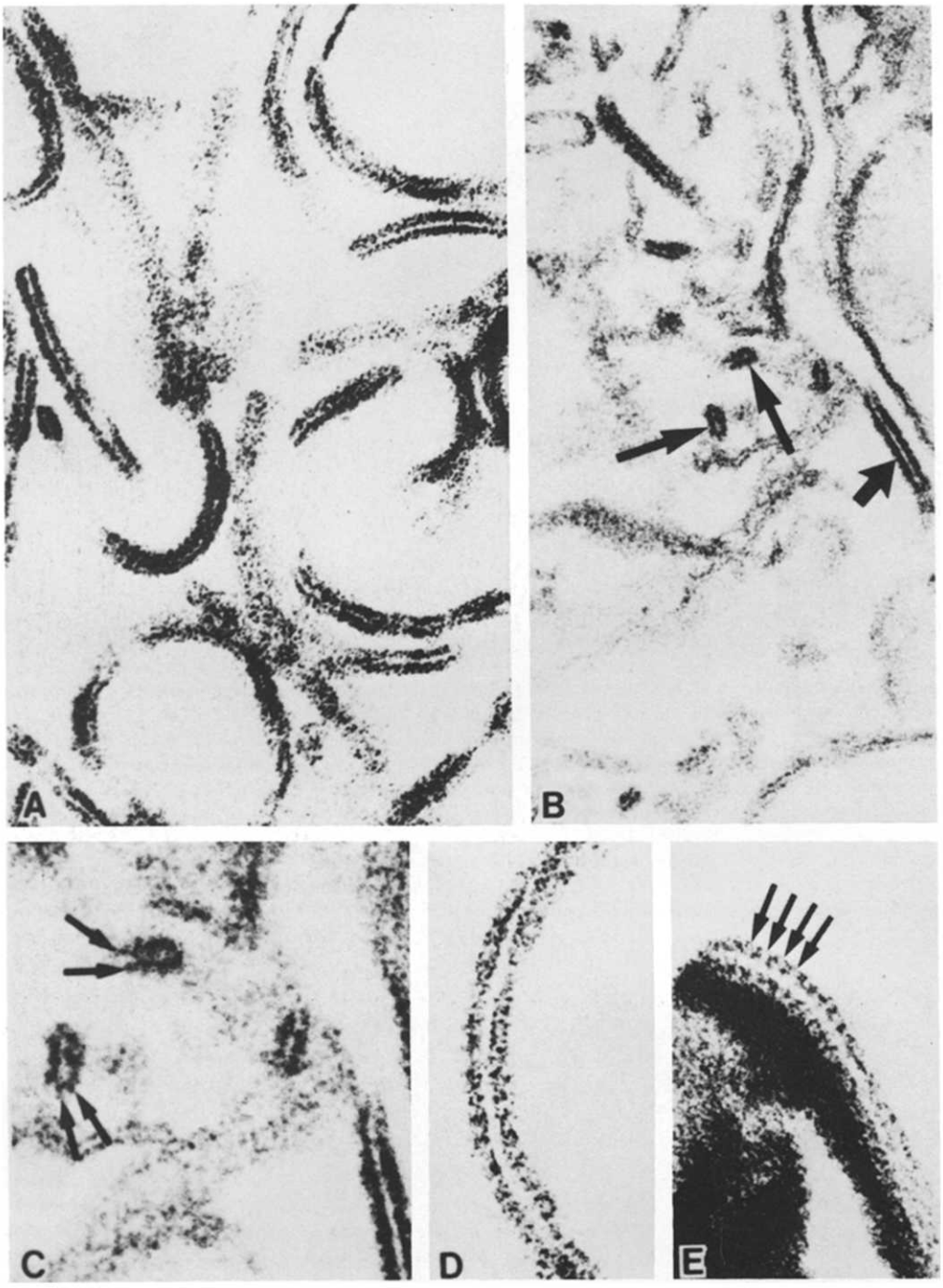

Fig. 5. Cylindrical polymers seen in thin sections. Low-magnification views of the cylinders sectioned at different angles are presented in panels A and B. Note the thick trilamellar structures in panel A. Elliptical structures that correspond to the cylinders sectioned transversely can be seen in panel B. Magnification: ×200000. Panel C presents higher magnification of the region at the center of panel B. The arrows label whiskers that correspond to the stalked particles described by negative staining (Figs. 1–4). The most common view of a transverse section through a cylinder is presented in panel D. Note the unstained core and the stained layers interrupted by clear regions which suggest the presence of organized material. Particles can be resolved if the section is well stained and the angle of viewing is adequate, and panel E shows such an image containing particles protruding from the core symmetrically (arrows). Note the similarity between these particles and those described in Figs. 2, 3 and 4. Magnification of panels C–E: ×400000.

opposite side, is seen in Fig. 4A (0° tilt). However, upon tilting, the particle at the right side both elongates and becomes more clearly distinguished. Thus its absence from Fig. 4A is due to the angle of the projection. In particular, an angle of tilt can be found (Fig. 4B, 20° tilt) where the particles at both sides of the unstained core give approximately equivalent appearances (arrowheads). If the tilt is then increased to 30° (Fig. 4D), the particle at the right side (arrowhead) remains distinct, whereas the one at the left side becomes difficult to distinguish because it has rotated so that its long axis is now oblique to the angle of view. Therefore, the different appearances presented by the particles are results of variations in the orientation or the 6 nm long particle with respect to the viewing angle of the microscope.

Changes in the appearance of the unstained core also occur upon tilting. The regions labelled with the arrows in panel A (0° tilt) are characterized by cores about 8 nm wide and layers of particles that are poorly defined. As the tilt is increased to 30° (Fig. 4D), the cores become significantly narrower (about 4 nm) and the layers of particles more distinct. Therefore, the fluctuations in the width of the central band seen in Figs. 2 and 3 arise from the twisting of an elliptical cylinder along its path. The decrease in the width of the core due to tilting, as well as the fluctuations in width along its length, can be explained if the cross-section of the central unstained core at any point is that of an ellipse with a minor-to-major axis ratio of about 1 : 2 and the two axes of the ellipse smoothly and slowly rotate along its length. The ellipticity of the core would also explain why larger deposits of stain accumulate in those regions where the core is thinnest (Fig. 2B, white arrow). Thus, the particles in the cylinder are tilted with respect to the major axis by about 30°.

Thin sectioning

The distinction between membrane fragments and cylinders by thin sectioning was complicated in that both structures displayed a similar appearance in transverse views. Nevertheless, we distinguished between these two structures by comparing their transverse views and their overall thickness. Fig. 5A shows a collection of curved structures displaying structural features similar to those previously described by negative staining (Figs. 1–4). The structures are about 15–16 nm in overall thickness, which is significantly larger than the thickness of a fragment of membrane. Like the cylinders seen in negatively stained preparations, these structures are constructed from an unstained central band about 4–5 nm wide having symmetrically arranged rows of poorly defined particles embedded in the layers of stain around them.

Cross-sections of the cylinders are seen as elliptical structures with an overall thickness of about

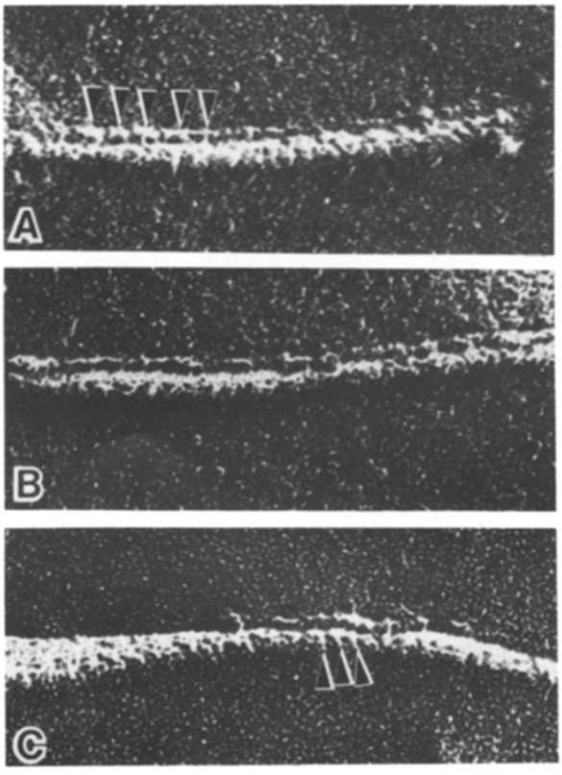

Fig. 6. Cylindrical aggregates observed by freeze-fracture-etching. In this experiment, isolated ($Na^+ + K^+$)-ATPase was fixed in glutaraldehyde and washed in distilled water before freezing. A small amount of water was sublimated from the fractured surface by etching at −105°C for 30 s. Panel A shows a surface of the tubule that contains discrete particles (arrowheads). Most often, the particles were distinguished as a thin line running parallel to the surface of the cylinder (panel B) separated by a narrow layer of platinum. In just a few cases we were to distinguish the symmetric arrangement of repeating material on the tubular surfaces (arrowheads in panel C). Magnification: ×320000.

10 nm along the minor axis and about 20–22 nm along the major axis (Fig. 5B). They contain an unstained core about 4 nm wide and layers of heavily stained material on their surfaces. The particles are better defined in the higher-magnification view shown in Fig. 5C. In this figure, the arrows label dense whiskers that are spaced about 6 nm apart and protrude from the surface of the unstained core.

Higher-magnification views of cylinders sectioned along their major axis frequently display curved structures about 15–16 nm in overall thickness comprised of a central band about 4 nm wide and layers of particles which are poorly resolved as discontinuities in the layers of stain (Fig. 5D). In a few instances (Fig. 5E), particles about 5–6 nm long and spaced about 5 nm apart can be resolved projecting from the unstained core.

Freeze-fracture-etch

Cylindrical structures were also seen in fracture surfaces that had been etched for 30 s to expose the underlying layers of particles (Fig. 6). These structures are comprised of a rounded core from which distinct particles of varying appearance protrude into the surrounding medium (arrows in Fig. 6A and C). The particles in Fig. 6A are about 9.5 nm by 3.5–4 nm and they are connected to the core by a narrow stalk. The particles in Fig. 6B appear as a thin line of density running parallel to the core and separated from it by a gap of about 4 nm. In Fig. 6C the particles protrude only on one side and appear as protrusions that can be traced to their insertion on the central band (arrowheads). Across from these protrusions a band of density runs parallel to the core separated by a narrow gap.

Discussion

Preparations of $(Na^+ + K^+)$-ATPase, purified by a widely used procedure, contain, in addition to fragments of membrane, long cylindrical structures (Fig. 1). The cylinders are formed from molecules of $(Na^+ + K^+)$-ATPase because the isolated preparations are of high purity and activity [21] and they are seen to originate from fragments of membranes studded with molecules of enzyme. Moreover, the particles seen constructing these cylinders have similar dimensions to those in the membrane fragments.

The views of these structures, when taken together, suggest that they are polymers constructed from rows of $(\alpha\beta)_2$ monomers. Although some of these cylinders might be constructed by the lateral association of several [3–5] rows of $\alpha\beta$ protomers, as suggested by cylinders with thicker cores (Fig. 2B), the large majority of them have a width consistent with an array of repeating $(\alpha\beta)_2$ dimers arranged as illustrated diagramatically in Fig. 7. From previous studies [18] it is known that each $\alpha\beta$ protomer of $(Na^+ + K^+)$-ATPase is about 12 nm in length, having a cytoplasmic domain (about 6 nm), a membrane-spanning domain (about 4 nm), and an extracellular domain (about 2 nm). The 6-nm particles that protrude from the core of the cylinders correspond to the cytoplasmic domain of the $(Na^+ + K^+)$-ATPase. The region that comprises the core of a cylinder could be constructed from the transmembrane domains, which should have very hydrophobic surfaces. The extracellular domains of the enzyme have not been resolved separately and identified within these structures.

The two views of the model in Fig. 7 can explain many of the structural details of the cylinder constructed by repeating $(\alpha\beta)_2$ dimers described in Figs. 1–6. To explain why some projections show particles on both sides of the core with equivalent appearance (Fig. 2) while others show particles on one side that are much shorter than those on the other (Fig. 3) and to explain how the projection changes upon rotation (Fig. 4), it is necessary to incline each $\alpha\beta$ protomer in the dimer at least 30° to the dyad axis of symmetry. By direct measurements of the micrographs and their optical transforms (Fig. 2), it is found that the particles on one side of a cylinder are staggered about 10° with respect to those on the other. Also, it can be shown that if the protomers had the same cross-section throughout their length (i.e., 4–5 nm) they would exhibit a stagger of 25°. To reconcile this difference we note that a smaller angle of stagger would result if the membrane-spanning domains of the protomers (where they are in direct contact) of the enzyme are narrower than the cytoplasmic domains. To account for the observed angle of 10°, the membrane-spanning domain

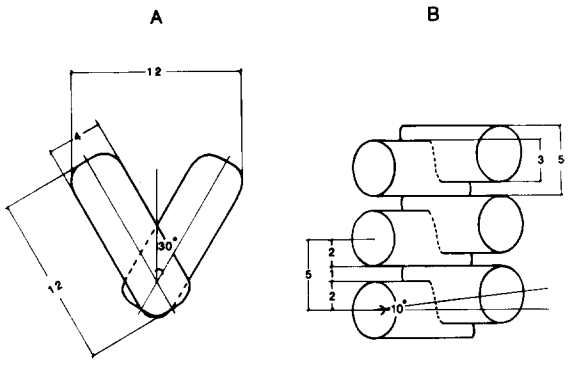

Fig. 7. Model of the structural organization of the cylindrical polymers of $(Na^+ + K^+)$-ATPase observed in the isolated fractions. The model proposes that each cylinder is constructed of a linear polymer of $(\alpha\beta)_2$ dimers of the enzyme. Panel A shows the front view of the model. The protomers are depicted as 12-nm-long particles inclined at 30° with respect to the axis passing through the middle of the polymer. The region where the protomers interact with their neighbors corresponds to the central band. The portions of the molecules protruding from the top surface correspond to the cytoplasmic domain. Panel B shows the top view of the model. The protomers from opposite rows are staggered by small angles. The model accounts for this fact by narrowing the cross-sectional area of the portion of the molecule that forms the central band (i.e., the membrane-spanning domain). In both views the lipid has been omitted to demonstrate better the orientation of the $(Na^+ + K^+)$-ATPase.

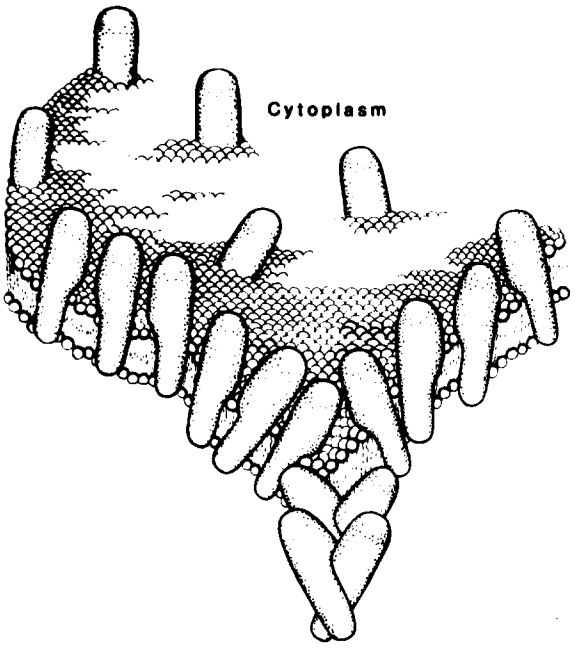

Fig. 8. A drawing of a cylinder of enzyme molecules connected to a membrane fragment. The open circles represent the polar head groups of the phospholipids and the larger structures represent $(Na^+ + K^+)$-ATPase molecules. The top surface corresponds to the cytoplasm. The lipid molecules have been omitted from the cylinders to illustrate the organization of the enzyme. The $\alpha\beta$ protomers of $(Na^+ + K^+)$-ATPase are placed tilted along the perimeter of the membrane fragments to minimize the hydrophobic free energy.

would have to be about 2.5–3 nm wide (Fig. 7B). The results of recent protein chemical experiments performed on $(Na^+ + K^+)$-ATPase also suggested that the membrane-spanning domain is significantly narrower than the cytoplasmic domain [33]. The unstained core of the cylinder formed from these membrane-spanning domains has dimensions of 4 nm by 2.5–3 nm, with the former being the dimension expected for the width of a lipid bilayer. Therefore, the cylinders do not represent edge-on views of membrane fragments as previously believed but a rather unique structure comprised of dimers of $(Na^+ + K^+)$-ATPase.

The question naturally arises as to how such structures can be formed. We propose that the cylinders are formed during homogenization, since they have not been seen in our studies of intact cells [27] and they are present prior to detergent purification. However, Repke [34], in a discussion of a paper, stated that similar cylinders were seen in kidney tubular cells. When tissues are homogenized, membrane fragments of irregular shapes are formed. These fragments are in an energetically unstable state, since nonpolar regions became exposed to the aqueous phase. In most membrane systems, the fragments minimize this hydrophobic energy by forming closed vesicles. Such is not the case for membrane containing large concentrations of $(Na^+ + K^+)$-ATPase where, after homogenization, single membrane fragments having cylinders attached to their perimeter are commonly found (Fig. 1A). Moreover, they are not observed in other membrane preparations displaying similar lipid/protein ratios such as liver gap junctions [35], lens gap junctions [36], purple membrane [37] and cytochrome oxidase [38], all of which form flat membrane fragments containing two-dimensional crystals of proteins. Thus, the ability to diminish the hydrophobic free energy at the perimeters and to form crystalline arrays is not unique to the $(Na^+ + K^+)$-ATPase. What is unique about this membrane-bound enzyme when compared to the

others is the strong tendency to form stable dimers. We suggest that it is this property of the enzyme that is responsible for the formation of the cylinders.

During homogenization, the plasma membrane is subject to large shear stresses which fragment it into irregular-shaped membrane pieces. Once the homogenization has ceased, these irregular-shaped fragments of membrane containing large numbers of enzyme molecules will tend to reduce their surface area to minimize the excess hydrophobic free energy. In the irregular, finger-like projections of plasma membrane, some enzyme molcules at both sides of the projection will spontaneously form dimers. We propose that this dimerization reaction may be the step that provides the nucleation center for growth of the cylinders. Simple analogies to this process are the closing of a zipper or the thinning of a black lipid film (see Fig. 8). Since nucleation sites might occur simultaneously at different points, cylinders can be interrupted along their length by pieces of membrane (see for example the region between the arrows in Fig. 3B) or have small pieces of membrane associated along their paths (Fig. 1B). In the transition region between the membranes and cylinders (arrows in Fig. 1A) there is a balance between the tension arising from the membrane curvature and the tension in the cylinder. The interactions tending to bring the molecules comprising the cylinder back into the membrane (to minimize the surface energy and increase the entropy of the enzyme molecules) is balanced by the energy necessary to dissociate the dimers. We note that the energy of dimerization must be considerable, since once the cylinders have formed they exist as stable entities and do not transform back into small membrane patches containing protomers.

The unexpected tendency of the $(Na^+ + K^+)$-ATPase to form stable and active linear arrays of $(\alpha\beta)_2$ dimers in the absence of cross-linking agents or detergents might resolve some of the conflicting information, obtained by chemical methods, concerning the quaternary structure of the native enzyme in the membrane-bound form. The consistent conversion of only a fraction of the total enzyme present in the preparations into products containing $(\alpha\beta)_2$ dimers reported in several studies [9,10] can now be explained as the result of the cross-linking of the dimers forming the cylinders. Therefore, our studies are consistent with the suggestion that it is the $\alpha\beta$ protomer which is responsible for enzymatic activity and that the formation of $(\alpha\beta)_2$ dimers is the result of a secondary, spontaneous aggregation which is independent of function.

Acknowledgements

We wish to thank Dr. N. Franks for helpful comments and Dr. W.A. Freytag for his interest in the problem and for providing us with the original fraction that showed the cylinders. We also thank James Gallagher for purifying the $(Na^+ + K^+)$-ATPase, and Carl Higgins for typing the manuscript. This work was supported by grants GM31845, GM33962 and NS20669 from the National Institutes of Health. We also acknowledge support from the MDA through the Jerry Lewis Neuromuscular Research Center grant and grant DMB-8413772 from the National Science Foundation.

References

1 Skou, J.C. (1969) Biochim. Biophys. Acta 42, 6–23
2 Kyte, J. (1971) J. Biol. Chem. 246, 4157–4165
3 Jørgensen, P.L. (1974) Biochim. Biophys. Acta 356, 36–52
4 Dixon, J.F. and L.E. Hokin (1974) Arch. Biochem. Biophys. 163, 749–758
5 Hokin, L.E., Dahl, J.L., Deupree, J.D., Dixon, J.F., Hackney, J.F. and Perdue, J.F. (1973) J. Biol. Chem. 248, 2593–2605
6 Kyte, J. (1972) J. Mol. Chem. 247, 7642–7649
7 Liang, S.M. and Winter, C.G. (1977) J. Biol. Chem. 252, 8278–8284
8 Craig, W.S. and Kyte, J. (1980) J. Biol. Chem. 255, 6262–6269
9 Kyte, J. (1975) J. Biol. Chem. 250, 7443–7449
10 Periyasami, S.M., Huang, W.H. and Askari, A. (1983) J. Biol. Chem. 258, 9878–9885
11 Kepner, G.R. and Macey, R.I. (1968) Biochim. Biophys. Acta 163, 188–203
12 Ellory, J.C., Green, J.R., Jarvis, S.M. and Young, J.D. (1979) J. Physiol. (Lond.) 295, 11–11P
13 Hasting, D.F. and Reynolds, J.A. (1979) Biochemistry 18, 817–821
14 Esmann, M. (1984) Biochim. Biophys. Acta 787, 81–89
15 Brotherus, J.R., Moller, J.V. and Jørgensen, P.L. (1981) Biochem. Biophys. Res. Commun. 100, 146–154
16 Craig, W.S. (1982) Biochemistry 21, 2667–2674
17 Craig, W.S. (1982) Biochemistry 21, 5707–5717

18 Skriver, E., Maunsbach, A.B. and Jørgensen, P.L. (1981) FEBSS Lett. 131, 219–222
19 Herbert, H., Jørgensen, P.L., and Skriver, E. and Maunsbach, A.V. (1982) Biochim. Biophys. Acta 689, 571–574
20 Mohraz, M. and Smith, P.R. (1984) J. Cell Biol. 98, 1836–1841
21 Zampighi, G., Kyte, J. and Freytag, W. (1984) J. Cell Biol. 98, 1851–1864
22 Jørgensen, P.L. and Skou, J.C. (1969) Biochem. Biophys. Res. Commun. 37, 39–46
23 Sealock, R. (1982) J. Cell Biol. 92, 514–522
24 Zampighi, G., Corless, J.M. and Robertson, J.D. (1980) J. Cell Biol. 86, 190–198
25 Erickson, H.P. and Klug, A. (1974) Phil. Trans. R. Soc. Lond. B. Biol. Sci. 261, 105–118
26 Salmon, E.D. and DeRosier, D. (1981) J. Microsc. (Oxf.) 123, 239–247
27 Zampighi, G. and Kreman, M. (1985) J. Membrane Biol., in the press
28 Costello, M.J. and Corless, J.M. (1978) J. Microsc. (Oxf.) 112, 17–37
29 Deguchi, N., Jørgensen, P.L. and Maunsbach, A.B. (1977) J. Cell Biol. 75, 619–634
30 Haase, J.W. and Kopspell, H. (1979) Pflugers Arch. 381, 127–135
31 Van Winkle, W.B., Lane, L.K. and Schwartz, A. (1976) Exp. Cell Res. 101, 291–296
32 Vogel, F., Meyer, H.W., Grosse, R. and Repke, H.R. (1977) Biochim. Biophys. Acta 470, 497–502
33 Nicholas, R.A. (1984) Biochemistry 23, 888–898
34 Repke, H.R. (1982) Proc. N.Y. Acad. Sci. 402, 265
35 Unwin, P.N.T. and Zampighi, G. (1980) Nature 283, 545–549
36 Zampighi, G., Simon, S.A., Robertson, J.D., McIntosh, T.J. and Costello, M.J. (1982) J. Cell Biol. 93, 175–189
37 Henderson, R. and Unwin, P.N.T. (1975) Nature 257, 28–32
38 Fuller, S.D., Capaldi, R.A. and Henderson, R. (1979) J. Mol. Biol. 134, 305–327